# Supporting Information

**Boosting the Oxygen Reduction Reaction Behaviour of Atomic Fe-$N_4$ Active Sites in the Porous Honeycomb-like Carbon *via* P Heteroatom Doping**

Jin Li [a], Kaicai Fan [b], Hongliang Jiang [c], Fenghong Lu [a], Lixiu Cui [a], Bin Li [b], Qi Zhang [a], Gao-Chao Fan [a, *], Lingbo Zong [a, *], Lei Wang [a,d, *]

a: Key Laboratory of Eco-chemical Engineering, College of Chemistry and Molecular Engineering, Qingdao University of Science and Technology, Qingdao 266042, China

b: College of Materials Science and Engineering, Qingdao University of Science and Technology, Qingdao 266042, China

c: Key Laboratory for Ultrafine Materials of Ministry of Education, School of Chemical Engineering, East China University of Science and Technology, Shanghai 200237, China

d: Shandong Engineering Research Centre of Marine Environment Corrosion and Safety Protection, College of Environment and Safety Engineering, Qingdao University of Science and Technology, Qingdao 266042, China

* Corresponding authors:

*E-mail addresses*: gcfan@qust.edu.cn; lingbozong@qust.edu.cn;

inorchemwl@126.com

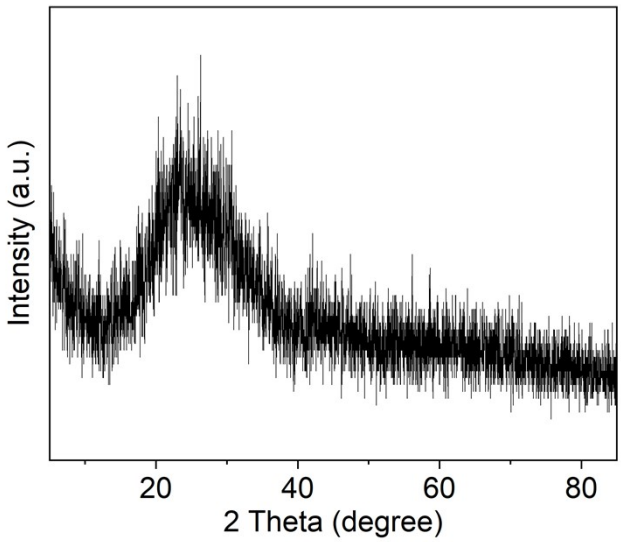


**Fig. S1.** The XRD pattern of Fe-$N_4$/NP-PHC.

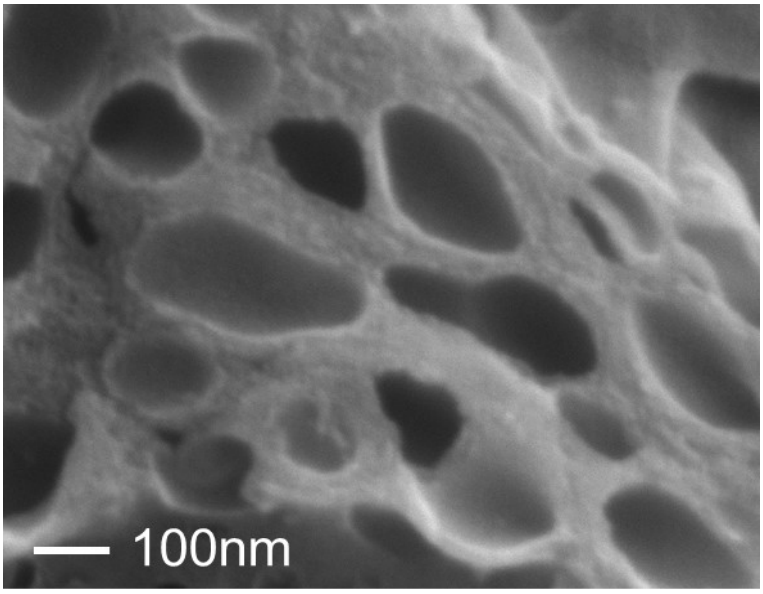


**Fig. S2.** SEM image of Fe-$N_4$/NP-PHC.

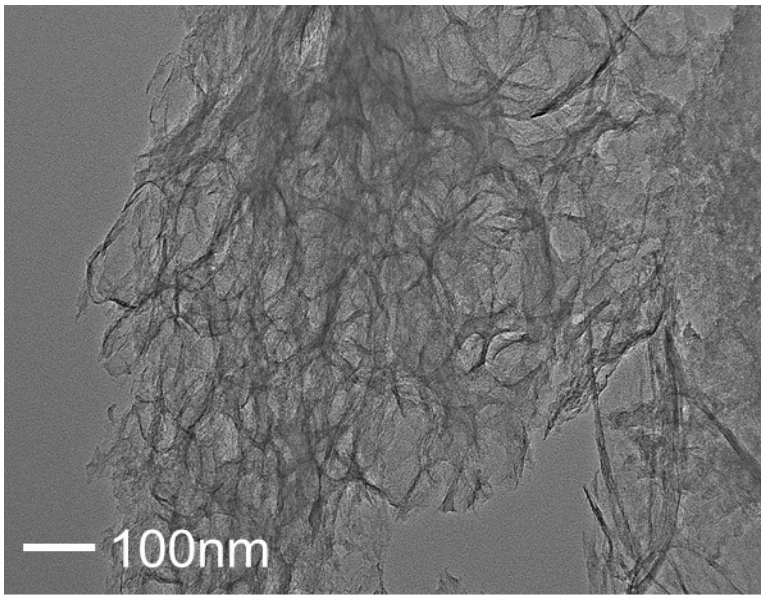


**Fig. S3.** TEM image of Fe-$N_4$/NP-PHC.

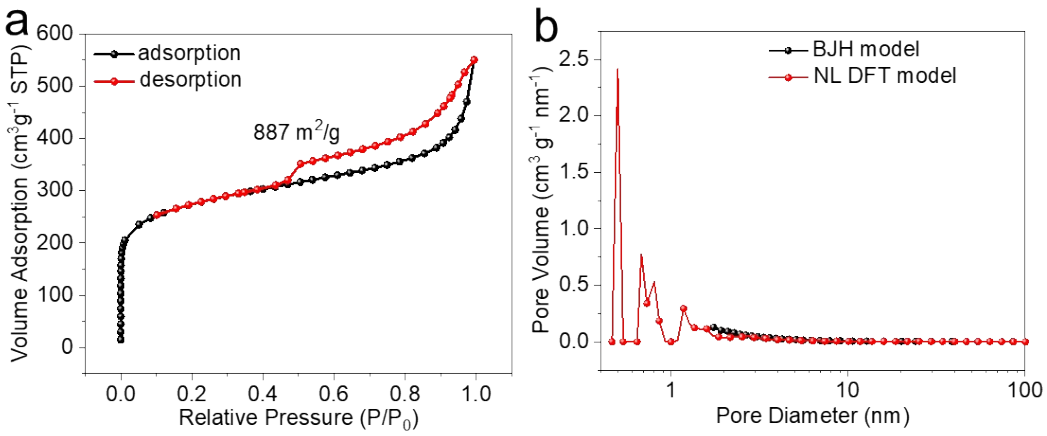


**Fig. S4.** $N_2$ adsorption-desorption isotherms and the corresponding pore distribution of Fe-$N_4$/NP-PHC.

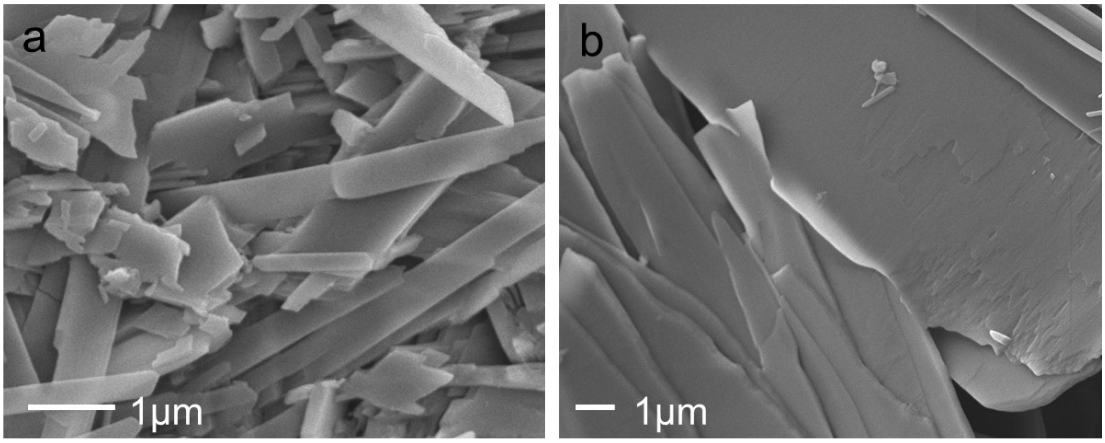


**Fig. S5.** SEM images of Fe-M-CA.

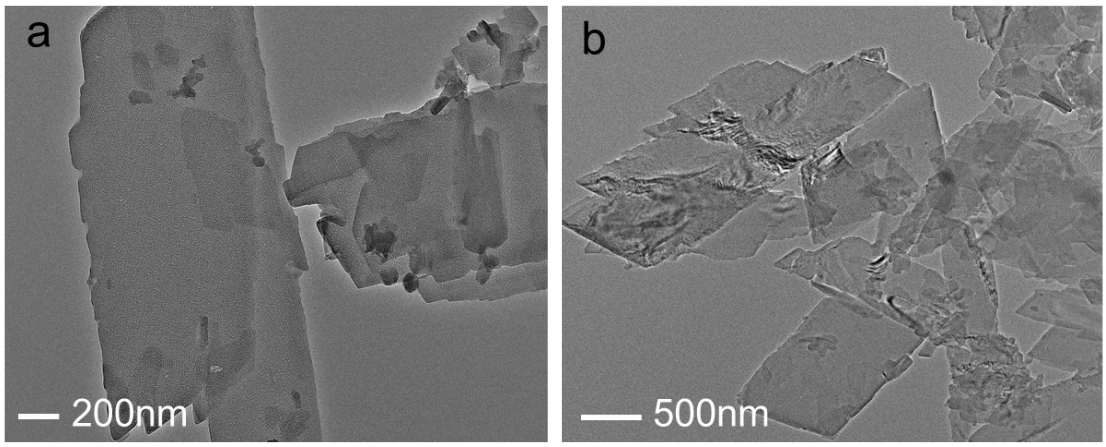


**Fig. S6.** TEM images of Fe-M-CA.

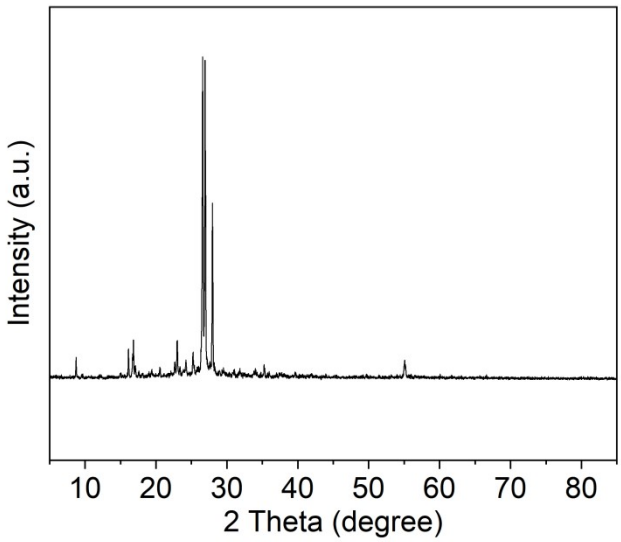


**Fig. S7.** XRD pattern of Fe-M-CA.

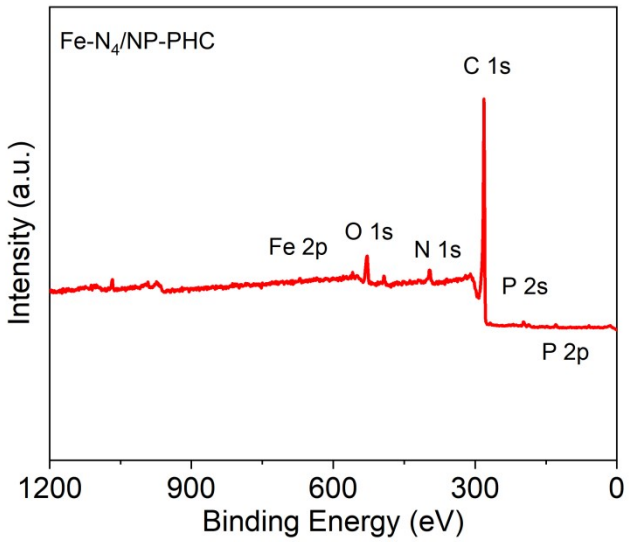


**Fig. S8.** The survey XPS spectra of Fe-$N_4$/NP-PHC.

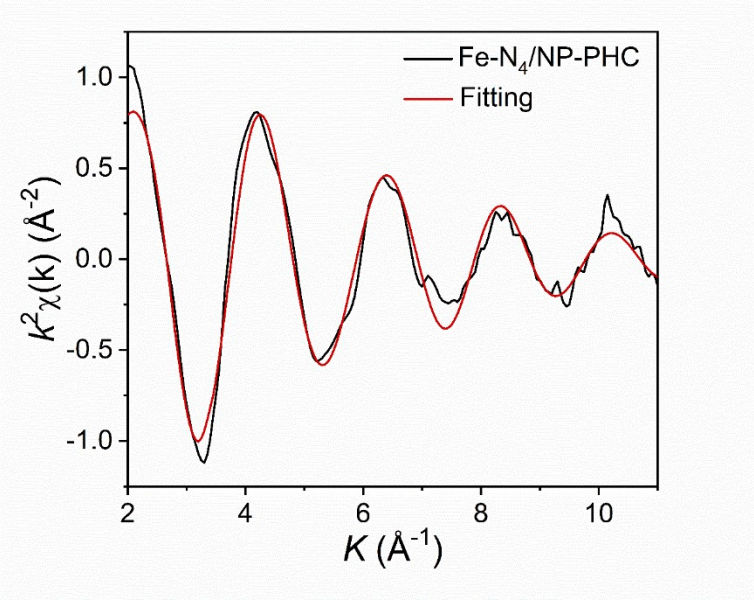


**Fig. S9.** EXAFS fitting results of Fe-$N_4$/NP-PHC at k space.

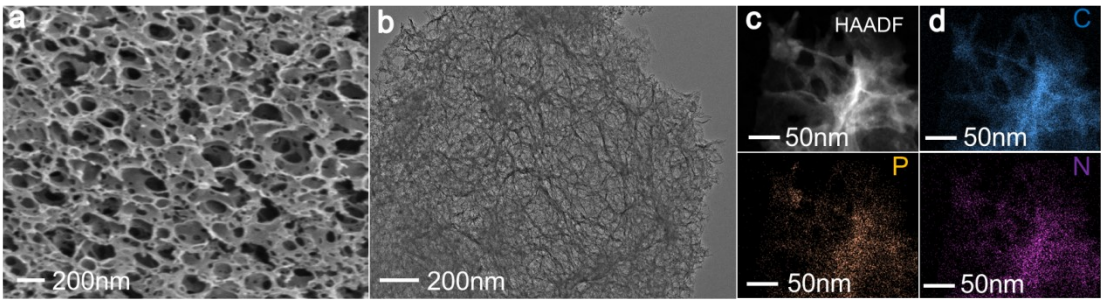


**Fig. S10.** (a) SEM and (b) TEM (c) HAADF-STEM and (d) elemental mapping images of NP-PHC.

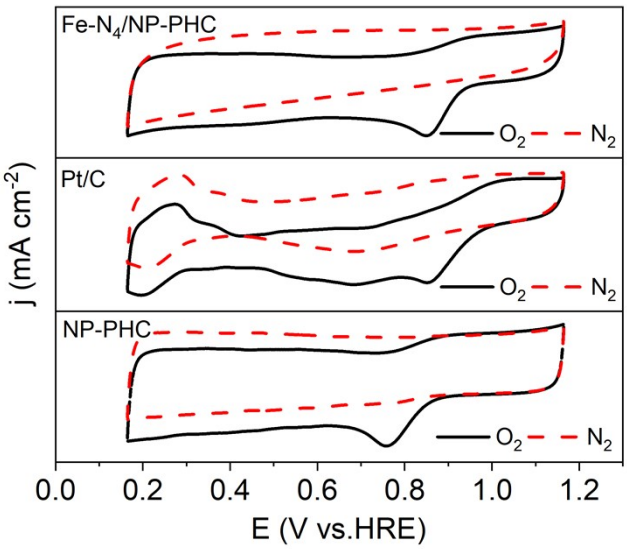


**Fig. S11.** CV curves of Fe-$N_4$/NP-PHC, Pt/C and NP-PHC.

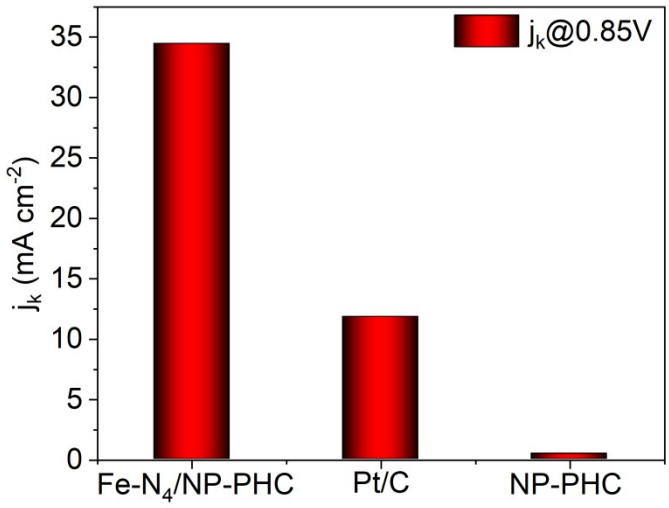


**Fig. S12.** Kinetic current density ($j_k$) of Fe-$N_4$/NP-PHC, Pt/C and NP-PHC at 0.85 V.

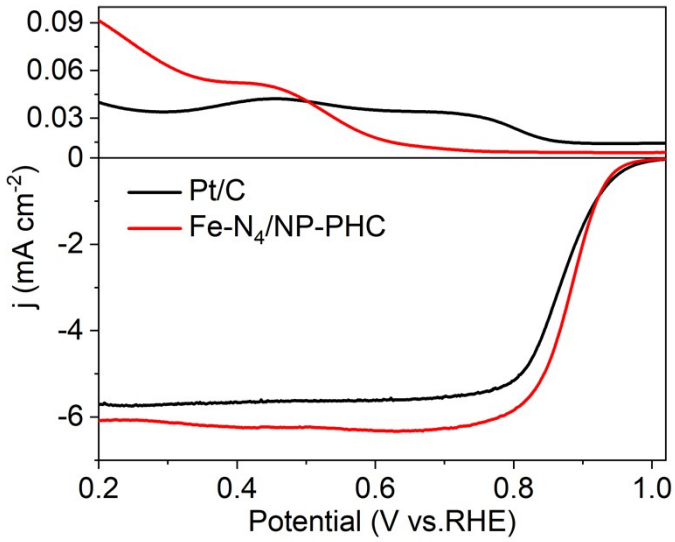


**Fig. S13.** Rotating ring disk electrode polarization curves of Fe-$N_4$/NP-PHC and Pt/C.

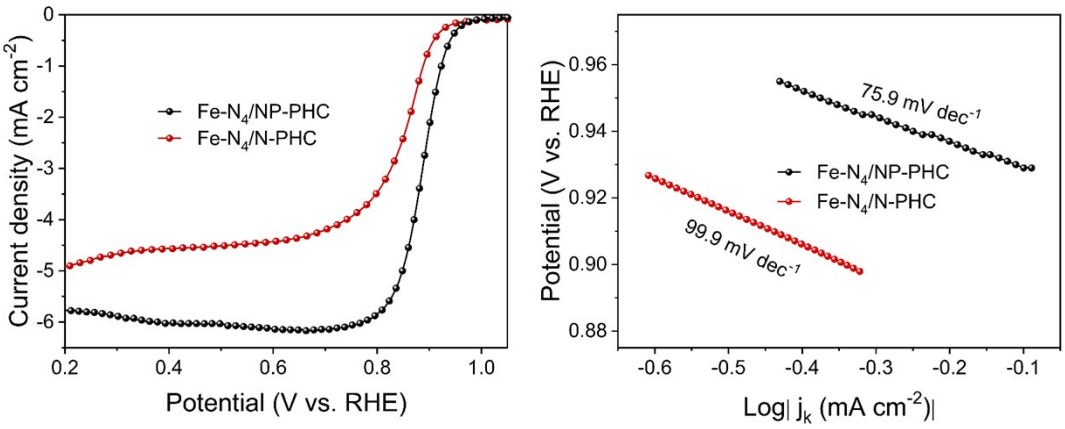


**Fig. S14.** (a) ORR polarization curves and (b) corresponding Tafel plots of Fe-$N_4$/NP-PHC and Fe-$N_4$/N-PHC.

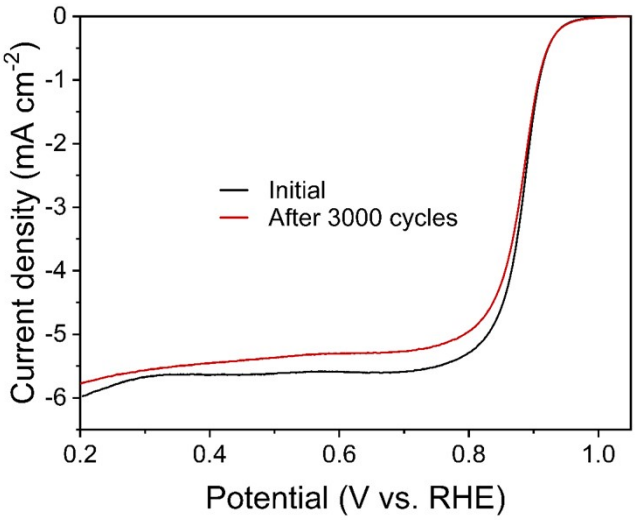


**Fig. S15.** ORR polarization curves before and after 3000 potential cycles for Fe-$N_4$/NP-PHC catalyst.

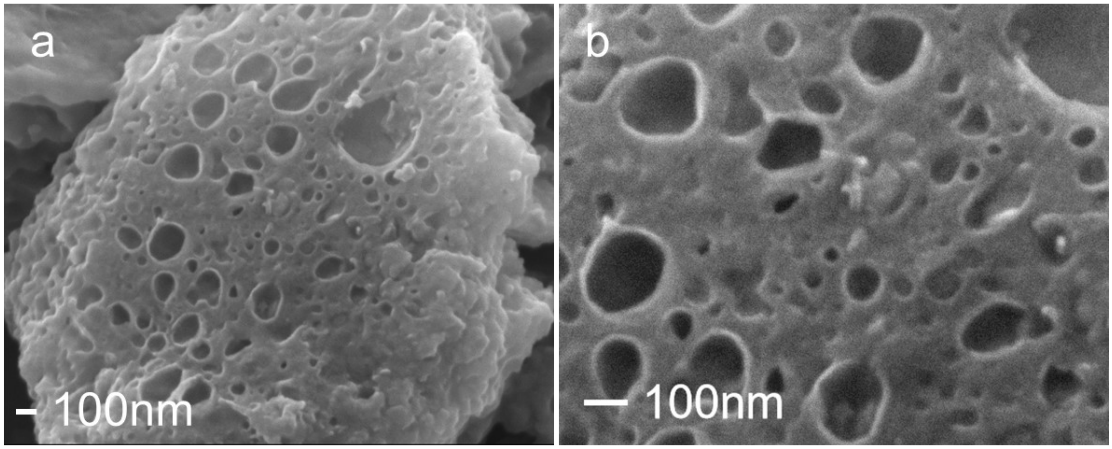


**Fig. S16.** SEM of Fe-$N_4$/NP-PHC after ORR durability measurement.

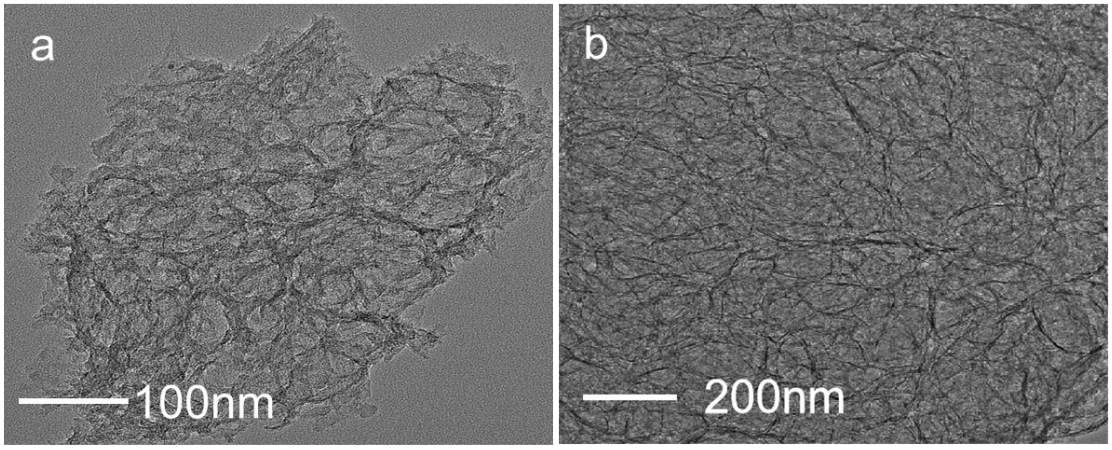


**Fig. S17.** TEM of Fe-$N_4$/NP-PHC after ORR durability measurement.

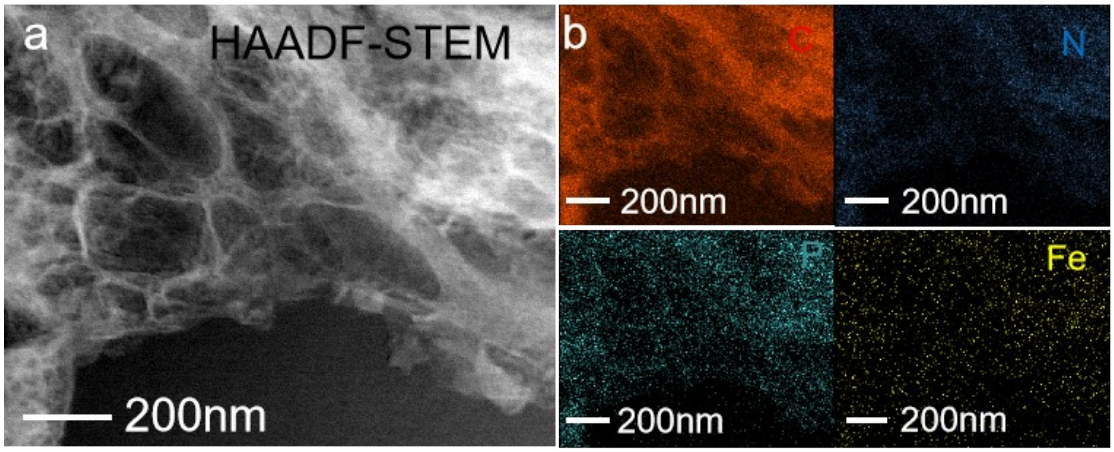


**Fig. S18.** (a) HAADF-STEM and (b) mapping images of Fe-$N_4$/NP-PHC after ORR durability measurement.

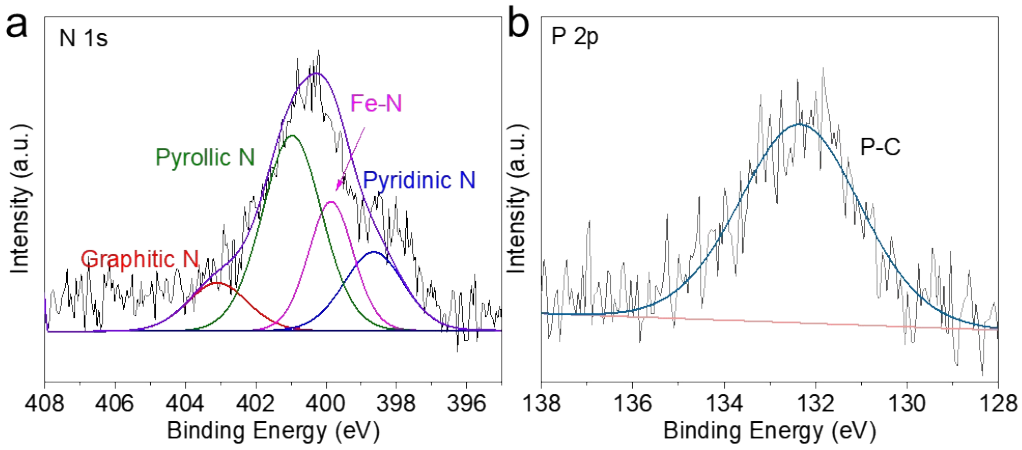


**Fig. S19.** XPS of Fe-$N_4$/NP-PHC after ORR durability measurement.

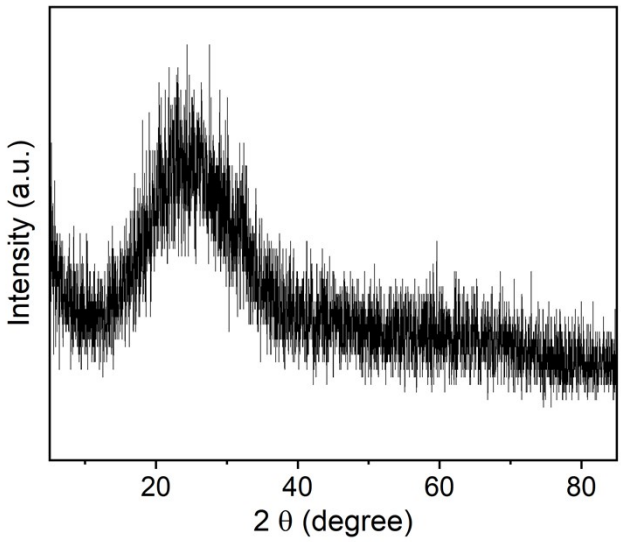


**Fig. S20.** XRD spectra of Fe-$N_4$/NP-PHC after stability test.

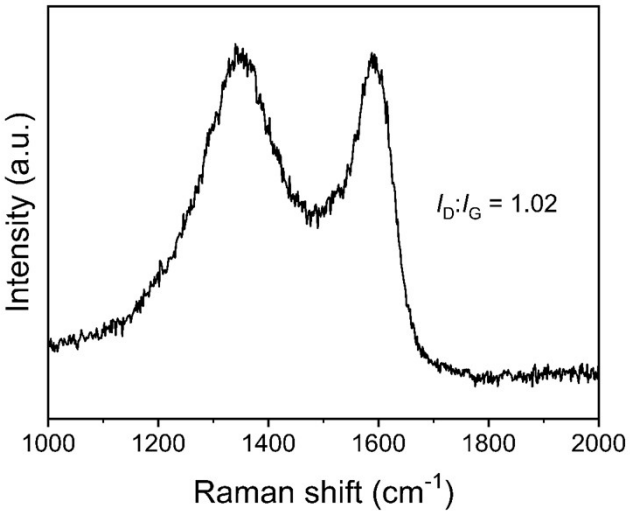


**Fig. S21.** Raman spectra of Fe-$N_4$/NP-PHC after stability test.

**Table S1.** Structural parameters extracted from EXAFS data fitting of ($S_0^2$ = 1)

| Samples | Shell | CN | R(Å) | $\sigma^2$ (Å$^2$) | $\Delta E_0$ (eV) | R-factor |
|---|---|---|---|---|---|---|
| Fe-$N_4$/NP-PHC | Fe-N | 4.1 | 2.01 | 0.006 | -4.58 | 0.012 |

CN is the coordination number; R is interatomic distance; $\sigma^2$ is Debye-Waller factor (a measure of thermal and static disorder); $\Delta E_0$: edge-energy shift (the difference between the zero kinetic energy value of the sample and that of the theoretical model); R factor is used to evaluate the goodness of the fitting.

**Table S2.** Performance of the reported state-of-the-art ORR SACs in 0.1 M KOH.

| Catalyst | $E_{onset}$(V vs.RHE) | $E_{1/2}$(V vs.RHE) | References |
|---|---|---|---|
| **Fe-$N_4$/NP-PHC** | **1.0 V** | **0.89V** | **This work** |
| Ni-$N_4$ | 0.97 V | 0.86 V | [1] |
| Fe/OES | 1.0 V | 0.85 V | [2] |
| FePc&rGO | 0.98 V | 0.89 V | [3] |
| Co-SAC/NC | 1.019 V | 0.884 V | [4] |
| Co-N-C SA/HCF | 0.928 V | 0.801 V | [5] |
| $Fe_3C$ | 0.987 V | 0.855 V | [6] |
| Co-$N_3C_1$ | 0.904 V | 0.824 V | [7] |
| FeSAs/PTF-600 | 1.01 V | 0.87 V | [8] |
| CNT@SAC-Co/NCP | -- | 0.87 V | [9] |
| SACe-N/PC | 1.0 V | 0.88 V | [10] |
| NBCNT-10 | 0.958 V | 0.82 V | [11] |
| CoFe/S-N-C | -- | 0.855 V | [12] |
| WN-Ni@N,P-CNT | 1.02 V | 0.84 V | [13] |
| Co,Nb-$MoS_2$/$TiO_2$ | 0.96 V | 0.86 V | [14] |
| 3DOM P-$Co_3O_{4-\delta}$ | 0.99 V | 0.82 V | [15] |
| $Co_9S_8$@N, S–C | 1.03 V | 0.887 V | [16] |
| PdNi/Ni@N-C | 1.01 V | 0.89 V | [17] |
| Fe-doped MOF CuCoSe@HCNF | -- | 0.756 V | [18] |
| Co/MnO@NC | 0.96 V | 0.83 V | [19] |

**Table S3.** Calculated ΔG for $4e^-$ ORR pathway on Fe-$N_4$ and Fe-$N_4$-P at U = 0 V vs. RHE.

| **U = 0 V** | **$O_2$ (eV)** | **OOH* (eV)** | **O* (eV)** | **OH* (eV)** | **$OH^-$ (eV)** |
|---|---|---|---|---|---|
| Fe-$N_4$/NP-CM | 4.92 | 3.39978 | 1.17276 | 0.1461 | 0.00 |
| Fe-$N_4$/N-CM | 4.92 | 3.2197 | 1.18296 | 0.05421 | 0.00 |

**Table S4.** Calculated ΔG for $4e^-$ ORR pathway on Fe-$N_4$ and Fe-$N_4$-P at U = 1.23 V (vs. RHE).

| **U = 1.23 V** | **$O_2$ (eV)** | **OOH* (eV)** | **O* (eV)** | **OH* (eV)** | **$OH^-$ (eV)** |
|---|---|---|---|---|---|
| Fe-$N_4$/NP-CM | 0 | -0.29022 | -1.28724 | -1.0839 | 0.00 |
| Fe-$N_4$/N-CM | 0 | -0.4703 | -1.27704 | -1.17579 | 0.00 |

**Table S5.** Performance of rechargeable Zn-air batteries assembled using SACs.

| Catalyst | Peak power density (mW $cm^{-2}$) | Charge/discharge voltage gap (V) at 10mA $cm^{-2}$ | Battery stability | References |
|---|---|---|---|---|
| **Fe-$N_4$/NP-PHC** | **200** | **1.0** | **20 min/cycle for 100 h** | **This work** |
| BCN/rGO-Co | 157 | 1.235 | for 200 h | [20] |
| Fe/N-G-SAC | 120 | 0.78 | 1 h/cycle for 240 h | [21] |
| $Ni_3Fe$/Co-N-C | 68 | 0.78 | for 65 h | [22] |
| Pt@CoS2-NrGO | 114 | 0.88 | for 55 h | [23] |
| CoNP-PTCOF | 53 | 1.2 | 10 min/cycle for 120 h | [24] |
| 3DOM Co3O4 | -- | 0.96 | 2 h/cycle for 400 h | [25] |
| Cop@CoNC | 188.8 | 0.80 | for 360 h | [26] |
| CoNP-s-IMCOF | 48 | 1.1 | 10 min cycle for 157h | [27] |
| P–CoO@PWC-2 | 73 | 0.83 | 20 min/cycle for 233.3 h | [28] |
| Fe-$Co_2P$@Fe-N-C | 81 | 0.73 | 40 min/cycle for 283.3 h | [29] |
| NiFe@C@Co CNFs | 130 | 0.73 | 20 min/cycle for 400 h | [30] |

References

[1] Z. Cai, P. Du, W. Liang, H. Zhang, P. Wu, C. Cai, Z. Yan, J. Mater. Chem. A, 2020, 8, 15012-15022.

[2] C.C. Hou, L. Zou, L. Sun, K. Zhang, Z. Liu, Y. Li, C. Li, R. Zou, J. Yu, Q. Xu, Angew. Chem. Int. Ed., 2020, 59, 7384-7389.

[3] Z.-y. Mei, S. Cai, G. Zhao, Q. Jing, X. Sheng, J. Jiang, H. Guo, Energy Storage Mater., 2022, 50, 12-20.

[4] P. Rao, J.M. Luo, D.X. Wu, J. Li, Q. Chen, P.L. Deng, Y.J. Shen, X.L. Tian, Energy & Environ. Mater. doi: 10.1002/eem2.12371

[5] J. Lei, H. Liu, D. Yin, L. Zhou, J.A. Liu, Q. Chen, X. Cui, R. He, T. Duan, W. Zhu, Small, 2020, 16, 1905920-1905929.

[6] M.M. Mohideen, A. V. Radhamani, S. Ramakrishna, Y. Wei, Y. Liu, J. Energy Chem., 2022, 69, 466-489.

[7] X. Hai, X. Zhao, N. Guo, C. Yao, C. Chen, W. Liu, Y. Du, H. Yan, J. Li, Z. Chen, X. Li, Z. Li, H. Xu, P. Lyu, J. Zhang, M. Lin, C. Su, S.J. Pennycook, C. Zhang, S. Xi, J. Lu, ACS Catal., 2020, 10, 5862-5870.

[8] Y. Zhou, G. Chen, Q. Wang, D. Wang, X. Tao, T. Zhang, X. Feng, K. Müllen, Adv. Funct. Mater., 2021, 31, 2102420-2102428.

[9] J.C. Li, Y. Meng, L. Zhang, G. Li, Z. Shi, P.X. Hou, C. Liu, H.M. Cheng, M. Shao, Adv. Funct. Mater., 2021, 31, 2103360-2103368.

[10] J.C. Li, X. Qin, F. Xiao, C. Liang, M. Xu, Y. Meng, E. Sarnello, L. Fang, T. Li, S. Ding, Z. Lyu, S. Zhu, X. Pan, P.X. Hou, C. Liu, Y. Lin, M. Shao, Nano Lett., 2021,

21, 4508-4515.

[11] P. Wei, X. Li, Z. He, X. Sun, Q. Liang, Z. Wang, C. Fang, Q. Li, H. Yang, J. Han, Y. Huang, Chem. Eng., 2021, 422, 130134-130143.

[12] G. Li, Y. Tang, T. Fu, Y. Xiang, Z. Xiong, Y. Si, C. Guo, Z. Jiang, Chem. Eng., 2022, 429, 132174-132181.

[13] Q. Zhang, F. Luo, X. Long, X. Yu, K. Qu, Z. Yang, Appl. Catal. B Environ., 2021,298, 120511-120519.

[14] D.C. Nguyen, T.L. Luyen Doan, S. Prabhakaran, D.T. Tran, D.H. Kim, J.H. Lee, N.H. Kim, Nano Energy, 2021, 82, 105750-105764.

[15] D. Wang, Y.-P. Deng, Y. Zhang, Y. Zhao, G. Zhou, L. Shui, Y. Hu, M. Shakouri, X. Wang, Z. Chen, Energy Storage Mater., 2021, 41, 427-435.

[16] D. Lyu, S. Yao, A. Ali, Z.Q. Tian, P. Tsiakaras, P.K. Shen, Adv. Energy Mater., 2021, 11, 2101249-2101261.

[17] Z. Li, H. Li, M. Li, J. Hu, Y. Liu, D. Sun, G. Fu, Y. Tang, Energy Storage Mater., 2021, 42, 118-128.

[18] S.-H. Chae, A. Muthurasu, T. Kim, J.S. Kim, M.-S. Khil, M. Lee, H. Kim, J.Y. Lee, H.Y. Kim, Appl. Catal. B Environ., 2021, 293, 120209-120220.

[19] Y. Niu, X. Teng, S. Gong, X. Liu, M. Xu, Z. Chen, Energy Storage Mater., 2021, 43, 42-52.

[20] L. Cao, Y. Wang, Q. Zhu, L.L. Fan, Y. Wu, Z.H. Li, S.X. Xiong, F. Gu, ACS Appl. Mater. Interfaces, 2022, 14, 17249−17258.

[21] M. Xiao, Z. Xing, Z. Jin, C. Liu, J. Ge, J. Zhu, Y. Wang, X. Zhao, Z. Chen, Adv.

Mater., 2020, 32, 2004900-2004908.

[22] J. Tan, T. Thomas, J. Liu, L. Yang, L. Pan, R. Cao, H. Shen, J. Wang, J. Liu, M. Yang, Chem. Eng., 2020, 395, 125151-125177.

[23] N. Logeshwaran, S. Ramakrishnan, S.S. Chandrasekaran, M. Vinothkannan, A.R. Kim, S. Sengodan, D.B. Velusamy, P. Varadhan, J.-H. He, D.J. Yoo, Appl. Catal. B Environ., 2021, 297, 120405-120416.

[24] J.H. Park, C.H. Lee, J.M. Ju, J.H. Lee, J. Seol, S.U. Lee, J.H. Kim, Adv. Funct. Mater., 2021, 31, 2101727-2101736.

[25] M.G. Park, D.U. Lee, M.H. Seo, Z.P. Cano, Z. Chen, Small, 2016, 12, 2707-2714.

[26] H. Yang, S.A. Gao, D.W. Rao, X.H. Yan, Energy Storage Mater., 2022, 46, 553-562

[27] J.-M. Ju, C. H. Lee, J. Hyun Park, J.-H. Lee, H.J. Lee, J.-H. Shin, S.-Y. Kwak, S. U. Lee, J.-H. Kim, ACS Appl. Mater. Interfaces DOI: 10.1021/acsami.2c04194

[28] H. Liu, Y. Liu, S. Mehdi, X. Wu, T. Liu, B. Zhou, P. Zhang, J. Jiang, B. Li, Adv. Sci., 2021, 8, 2101314-2101325.

[29] X.W. Lv, W.S. Xu, W.W. Tian, H.Y. Wang, Z.Y. Yuan, Small, 2021, 17, 2101856-2101868.

[30] X. Chen, J. Pu, X.H. Hu, Y.C. Yao, Y.B. Dou, J.J. Jiang, W.J. Zhang, Small, 2022, 18, 2200578-2200589.